


Cite this: *RSC Adv.*, 2018, 8, 20287

Ag decorated silica nanostructures for surface plasmon enhanced photocatalysis†

Ratyakshi Nain,^a Saiyam Dobhal,^a Parth Bidaliya,^a Gajender Saini,^b Balaram Pani ^{*a} and Sidhharth Sirohi^{*a}

In this article, we present a novel synthesis of mesoporous SiO₂/Ag nanostructures for dye (methylene blue) adsorption and surface plasmon mediated photocatalysis. Mesoporous SiO₂ nanoparticles with a pore size of 3.2 nm were synthesized using cetyltrimethylammonium bromide as a structure directing agent and functionalized with (3-aminopropyl)trimethoxysilane to introduce amine groups. The adsorption behavior of non-porous SiO₂ nanoparticles was compared with that of the mesoporous silica nanoparticles. The large surface area and higher porosity of mesoporous SiO₂ facilitated better adsorption of the dye as compared to the non-porous silica. Ag decorated SiO₂ nanoparticles were synthesized by attaching silver (Ag) nanoparticles of different morphologies, *i.e.* spherical and triangular, on amine functionalized silica. The photocatalytic activity of the mesoporous SiO₂/Ag was compared with that of non-porous SiO₂/Ag nanoparticles and pristine Ag nanoparticles. Mesoporous SiO₂ nanoparticles ($k_d = 31.3 \times 10^{-3} \text{ g mg}^{-1} \text{ min}^{-1}$) showed remarkable improvement in the rate of degradation of methylene blue as compared to non-porous SiO₂ ($k_d = 25.1 \times 10^{-3} \text{ g mg}^{-1} \text{ min}^{-1}$) and pristine Ag nanoparticles ($k_d = 19.3 \times 10^{-3} \text{ g mg}^{-1} \text{ min}^{-1}$). Blue Ag nanoparticles, owing to their better charge carrier generation and enhanced surface plasmon resonance, exhibited superior photocatalysis performance as compared to yellow Ag nanoparticles in all nanostructures.

Received 23rd March 2018

Accepted 28th May 2018

DOI: 10.1039/c8ra02543f

rsc.li/rsc-advances

Introduction

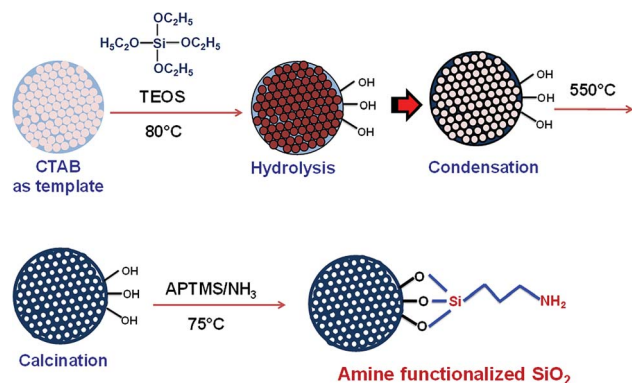
Synthetic dyes, having complex aromatic structures, are primary pollutants of various industries including textile, food, cosmetics, printing, electronics, paper, rubber, *etc.*¹ These dyes and their degradation products, being carcinogenic and mutagenic, are hazardous to the environment. Various physical and chemical procedures have been developed for treatment of industrial waste-water containing dyes before their disposal into the environment. The best employed method is adsorption, owing to the simple design and effectiveness in removal of dyes without resulting any harmful residues. Moreover, the recyclable nature of the adsorbents makes the process energy and cost effective also. A variety of adsorbents have been explored for removal of dyes such as silica,^{2,3} magnetic nanoparticles,⁴ activated carbon,⁵ zeolites,⁶ *etc.* The adsorption process is influenced by numerous factors including surface area of adsorbent, and extent and type of interaction of the dye with the adsorbent.⁷

Mesoporous silica, due to its large surface area, high hydrothermal stability, and diverse surface functionality, has been explored extensively for biomedical applications, namely cell imaging, diagnosis, biosensing, intracellular drug delivery^{8–15} and controlled pesticide release.¹⁶ The presence of silanol groups ensures better adsorption of dye molecules on its surface.¹⁷ Researchers have investigated photocatalytic activity of various nanoparticles (NPs) including TiO₂,¹⁸ ZnO,^{19,20} MnO₂,²¹ Silver,²² *etc.* The optical spectra of metallic nanoparticles are dominated by Surface Plasmon Resonance (SPR), which is due to collective oscillation of conduction electrons. Silver nanoparticles (AgNPs) possess intense SPR, which is of great advantage for Surface Enhanced Raman Spectroscopy (SERS) and sensing applications. Recently AgNPs have been proposed as a novel photocatalyst for degradation of organic pollutants due to their SPR absorption in the visible range. Ag NPs, when excited with photon, energize conduction electrons of 5sp bands and excite them to higher-energy states. These excited electrons participate in chemical reactions.²³ Additionally, holes left behind in the 5sp bands possess strong oxidizing power, and therefore act as driving force for photocatalysis. SPR frequency of Ag is a function of its particle size and shape. The Ag/SiO₂ nanostructures with Ag as core material have been explored for sensing,^{24,25} antibacterial²⁶ and SERS²⁷ applications. Yellow AgNPs decorated non-porous SiO₂/Ag core shell nanostructures have been investigated for plasmon mediated

^aBhaskaracharya College of Applied Sciences, University of Delhi, Delhi-110075, India.
E-mail: balarampani63@gmail.com; sidbcas@gmail.com

^bCRNTS, IIT-Mumbai, Maharashtra-400076, India

† Electronic supplementary information (ESI) available: SEM micrographs of non-porous and mesoporous silica and FTIR of amine functionalized silica. See DOI: 10.1039/c8ra02543f



Scheme 1 Synthesis and functionalization of mesoporous silica nanoparticles.

photocatalysis.²⁸ On account of better charge carrier generation, blue AgNPs may improve photocatalytic performance of SiO₂/blue Ag nanostructures in a significant manner. The large surface area of mesoporous SiO₂ will further facilitate adsorption and hence catalysis.²⁹

In the present work, we have made an attempt to synthesize mesoporous SiO₂/Ag composite nanostructures. The adsorption behavior of non-porous silica (SiO₂) and mesoporous silica (MS-SiO₂) towards methylene blue dye has been investigated. Amine functionalized silica was then used for adsorption of AgNPs on its surface. The synthesized SiO₂/Ag composite nanostructures were compared with pristine AgNPs for their photocatalytic behavior against methylene blue. The effect of porosity of silica and shape of AgNPs on photocatalysis was also investigated. MS-SiO₂/Ag composite nanostructures are expected to have better adsorption of dye due to large surface area and porosity of mesoporous silica. The dye degradation process may get accelerated by plasmon assisted photocatalysis of Ag nanoparticles.

Experimental

Materials

The chemicals used were tetraethylorthosilicate (TEOS, ≥99%) (Merck, India), *N,N,N*-cetyltrimethylammonium bromide (CTAB) (Merck, India), (3-aminopropyl)trimethoxysilane (APTMS, 95%) (Merck, India), NaOH (Merck, India), NaBH₄ (Merck, India), 30% w/v H₂O₂ (Merck, India), silver nitrate (Merck, India), sodium citrate (Merck, India), methylene blue (CDH, India), ethanol (Merck, India), 25% (w/v) NH₃ solution (≥99%) (Fisher, India), poly(vinyl pyrrolidone) (*M_w* 40 000, CDH, India) and sodium

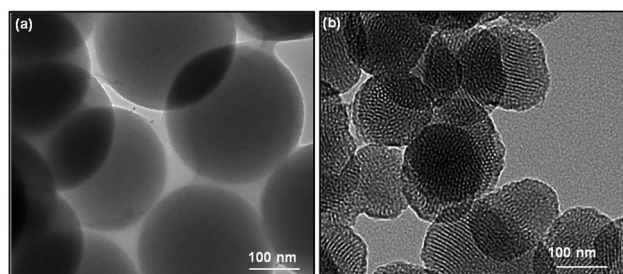


Fig. 1 HRTEM micrographs of (a) SiO₂ (b) MS-SiO₂.

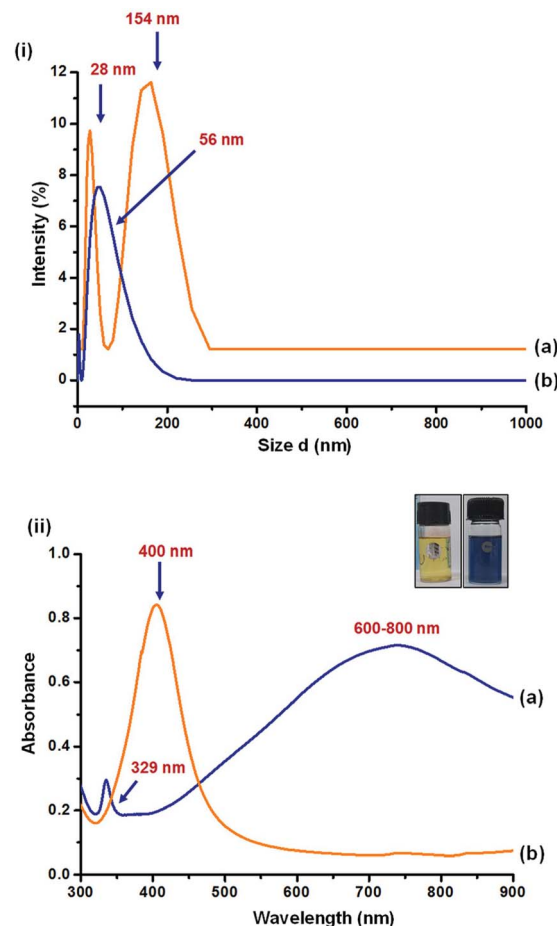


Fig. 2 (i) Particle size analysis and (ii) UV-Vis spectra of (a) yellow Ag and (b) blue Ag.

dodecyl sulphate (SDS) (Merck, India). All the used chemicals were of analytical grade and used as received. Double deionized water was used in all the synthesis processes. All glassware items were first rinsed with *aqua regia* and thoroughly with deionized water followed by acetone before use.

Methods

Synthesis of non-porous silica nanoparticles using Stober method. Silica nanoparticles were prepared by the Stober method. In brief, the precursor solution was prepared by adding 0.5 mL TEOS to 2 mL ethanol. The TEOS/ethanol solution was then added to a solution of 100 mL ethanol and 25 mL aqueous ammonia and stirred for 2 h at 40 °C. 8 mL of TEOS diluted with

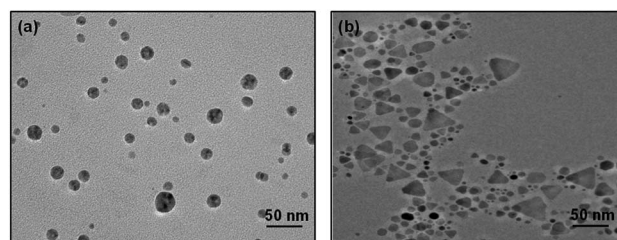


Fig. 3 HRTEM images of (a) yellow Ag and (b) blue Ag.



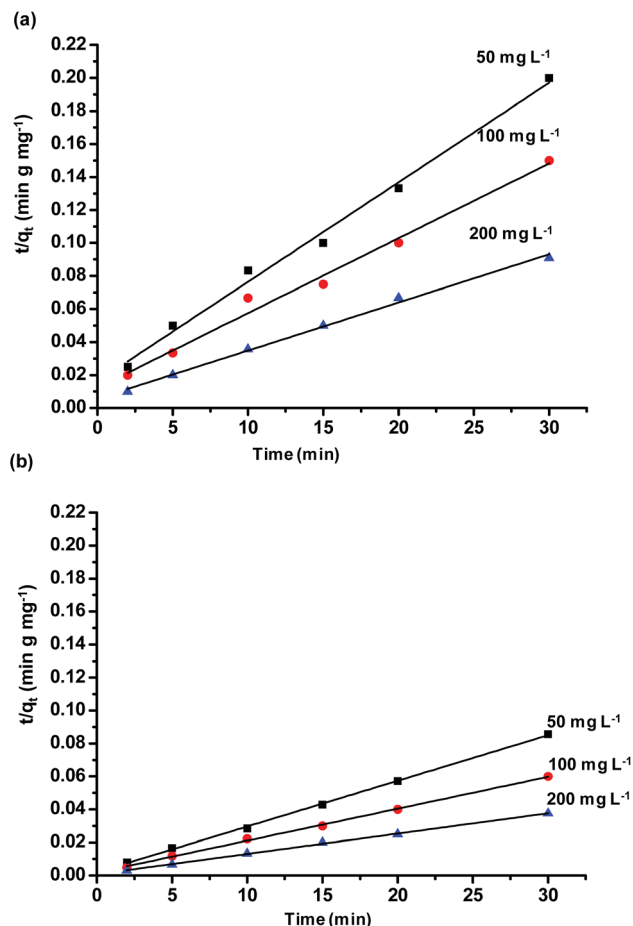


Fig. 4 Effect of dye concentration on adsorption rate constant (k_a) (a) SiO₂ (b) MS-SiO₂ silica.

32 mL ethanol was added in the above prepared solution and stirred for 2 h. Reaction mixture was then centrifuged at 5000 rpm and washed with water followed by ethanol. The precipitates were vacuum dried at 55 °C for 24 h followed by calcination at 450 °C for 2 h.

Synthesis of mesoporous silica nanoparticles. Mesoporous silica nanoparticles were synthesized using CTAB as structure directing agent and TEOS as precursor as reported by Cao *et al.*¹⁶ with a little modification. Briefly, 73 μ L of 2 M NaOH (0.156 μ moles), and 0.0221 g (60.6 μ moles) of CTAB were dissolved in 10 mL of deionized water with stirring for 30 minutes at ambient temperature. The temperature was increased to 80 °C in an oil bath, and subsequently 104 μ L of TEOS were added drop wise. The reaction time was kept 75 min. Reaction mixture was then centrifuged at 2000 rpm and washed with water followed by ethanol. The precipitates were vacuum dried at 55 °C for 24 h followed by calcination at 550 °C for 5 h.

The morphology of obtained nanoparticles was analyzed using field emission scanning electron microscope (FE-SEM) (FEI Quanta 200F, Netherland) and high resolution transmission electron microscope (HRTEM) (JEM 2100F, JEOL, Tokyo Japan). Diameter of the nanoparticles was determined as an average of 200 readings using ImageJ software. Fourier Transform Infrared Spectroscopy (FTIR) (Bruker-Alpha, USA)

was used for chemical structure characterization. The porous nature of the product was analyzed using N₂ adsorption/desorption isotherms on Micromeritics ASAP 2010 Accelerated Surface Area and Porosity Analyzer. Data was evaluated using the BET method to calculate the surface area and pore size distribution, respectively.

Synthesis of silver nanoparticles. For the synthesis of silver nanoparticles, poly(vinyl pyrrolidone) (PVP) and sodium citrate were used as capping agent and H₂O₂ as etching agent. In a typical synthesis, 0.002 mmol of silver nitrate and 0.0092 mmol of PVP were dissolved in 50 mL of DI water at 60 °C. 900 μ L of 30% H₂O₂ and 0.0551 mmol of sodium citrate were added to the solution with continuous stirring at 500 rpm. 900 and 500 μ L of 0.177 mM solution of sodium borohydride were added into above prepared mixture of silver nitrate for synthesis of blue and yellow Ag, respectively. The reaction mixture was stirred for 30 minutes at 500 rpm. The obtained silver nanoparticles were characterized using UV spectrophotometer (Lambda 35, Perkin elmer, USA), particle size analyzer (Malvern Zetasizer Nano ZS, USA) and high resolution transmission electron microscope (HRTEM).

Functionalization of silica nanoparticles. The obtained silica nanoparticles were functionalized using APTMS. In a typical procedure 0.5 g of silica nanoparticles were dispersed in 5 mL of ammonia solution (25% w/v). 10% (v/v) of APTMS dissolved in chloroform was added drop wise to the above dispersion and kept for 1 h at 75 °C. Functionalized silica particles thus obtained were centrifuged and dried in vacuum oven 55 °C for 24 h for further use.

Adsorption of dye using non-porous and mesoporous silica nanoparticles. Solutions of 50, 100 and 200 mg L⁻¹ methylene blue were prepared in DI water. The dye solutions were then used for adsorption study of both non-porous and mesoporous silica nanoparticles. The samples were analyzed using UV spectrophotometer and adsorption rate constant was calculated for each concentration.

Photocatalysis of methylene blue. 0.5 g of silica particles were dispersed in 5 mL of silver colloidal solution by stirring for 15 min followed by ultrasonication for 15 min and centrifugation at 5000 rpm. SiO₂/Ag composite nanostructures settled down leaving behind the clear supernatant and were coded as

Table 1 Effect of dye concentration on k_a for silica and mesoporous silica

	Concentration of dye (mg L ⁻¹)		
	50	100	200
SiO₂			
k_a (g mg ⁻¹ min ⁻¹ $\times 10^{-3}$)	2.21	1.66	1.45
q_e Cal (mg g ⁻¹)	166	222	344
q_e Exp (mg g ⁻¹)	150	200	330
MS-SiO₂			
k_a (g mg ⁻¹ min ⁻¹ $\times 10^{-3}$)	3.92	2.01	1.8
q_e Cal (mg g ⁻¹)	357	526	833
q_e Exp (mg g ⁻¹)	350	500	800



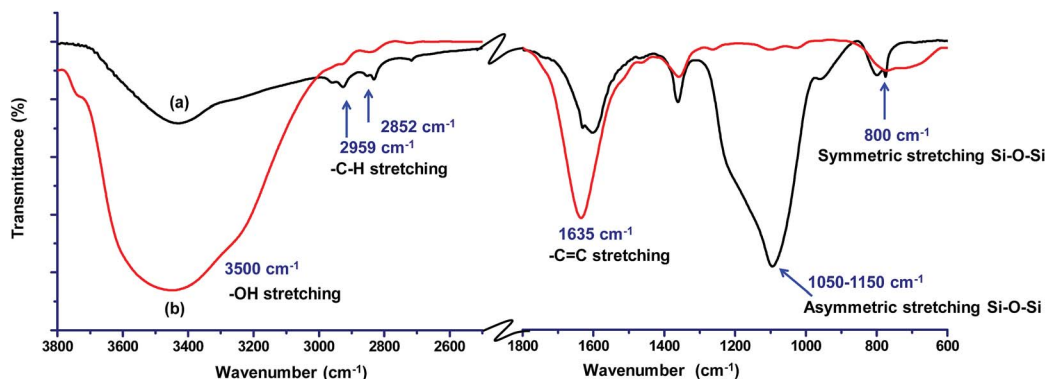
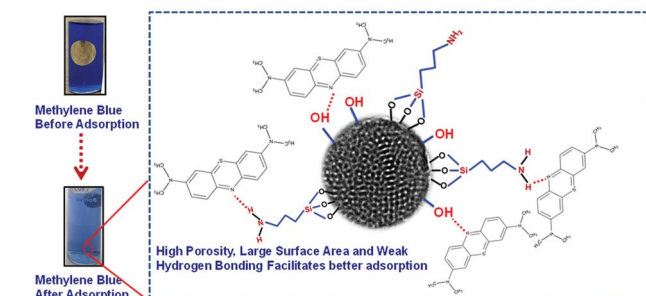


Fig. 5 FTIR spectra of (a) amine functionalized MS-SiO₂ nanoparticles and (b) dye adsorbed amine functionalized MS-SiO₂ nanoparticles.



Scheme 2 Mechanism of dye adsorption by amine functionalized MS-SiO₂.

SiO₂/Ag and MS-SiO₂/Ag for non-porous and mesoporous silica nanoparticles, respectively. The nanostructures were dried in vacuum oven and examined using HRTEM and EDX. Pristine, SiO₂/Ag and MS-SiO₂/Ag nanostructures were compared for their photocatalysis behavior using 200 mg L⁻¹ methylene blue. For the study, 0.2% (w/v) of nanostructures were dispersed in methylene blue solution. The methylene blue solution with nanostructures was kept in dark to attain the adsorption/desorption equilibrium and then exposed to the sunlight for

photodegradation. The photocatalytic behavior was analyzed using UV spectrophotometer (Scheme 1).

Results and discussion

Morphology of SiO₂ and MS-SiO₂ nanoparticles

The morphology of obtained SiO₂ nanoparticles was analyzed using scanning electron microscope (SEM) and high-resolution transmission electron microscope (HRTEM). The SEM micrographs of non-porous silica (SiO₂) and mesoporous silica (MS-SiO₂) are shown in Fig. S1.† SEM analysis revealed that SiO₂ and MS-SiO₂ nanoparticles were of spherical shape with an average diameter of 250 ± 30 and 100 ± 12 nm respectively. HRTEM micrographs established the porous nature of the mesoporous silica (Fig. 1) with an estimated pore size of 3.0 ± 0.05 nm. This was further confirmed using BET analysis and the calculated surface area and adsorption average pore diameter was found to be 265 ± 10 m² g⁻¹ and 3.2 nm respectively.

FTIR spectra of amine functionalized mesoporous silica nanoparticles are shown in Fig. S2.† The stretching vibrations of hydrogen-bonded Si-OH group, -OH of physically adsorbed water molecules and -NH₂ groups were found as a broad peak at 3425 cm⁻¹. The new peaks at 2959, 2852 and 1633 cm⁻¹ were attributed to asymmetric and symmetric -C-H stretching of aminopropyl and -NH₂ bending vibrations respectively.³⁰ Splitting of Si-O-Si symmetric stretching peak at 772 cm⁻¹ further confirmed interaction of Si-O-Si with -NH₂ groups.

Characterization of silver nanoparticles

Particle size analysis and UV-Vis spectra of Ag NPs are shown in Fig. 2. The yellow AgNPs were found to have a narrow and

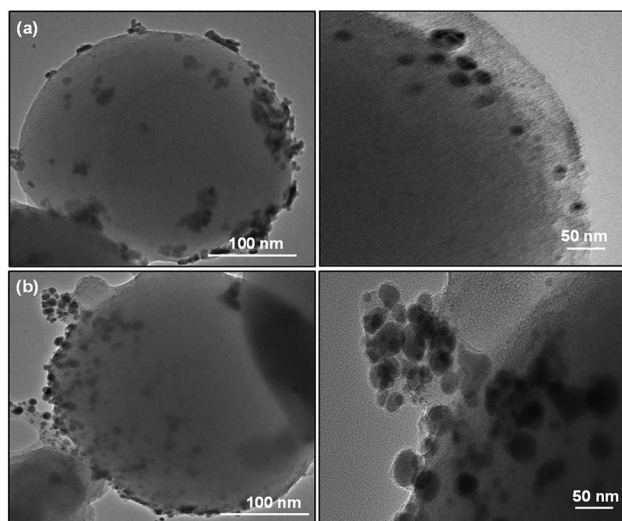


Fig. 6 HRTEM images of (a) SiO₂/yellow Ag and (b) SiO₂/blue Ag.

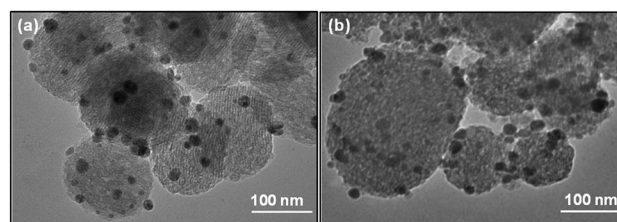


Fig. 7 HRTEM images of (a) MS-SiO₂/yellow Ag and (b) MS-SiO₂/blue Ag.



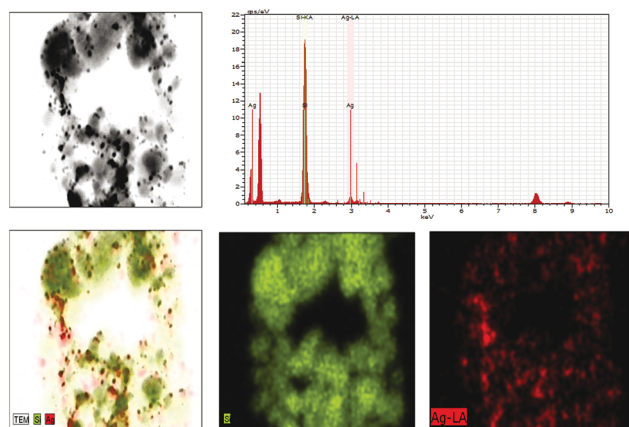


Fig. 8 EDX mapping of MS-SiO₂/blue Ag.

small peak at 28 nm and a broad peak at 154 nm. The peak corresponding to 154 nm may be attributed to the aggregated AgNPs. The smaller size and high surface energy could result in larger aggregates. On the other hand, single peak corresponding to 56 nm was observed for blue Ag NPs.

UV-Vis spectra of the particles resemble with literature. Yellow AgNPs, being spherical in shape, were found to have in-plane dipole plasmon resonance peak at 400 nm. As reported in literature³¹ the in-plane dipole plasmon resonance of blue AgNPs was observed at 600–800 nm. An additional peak at 329 nm and a hump at 470 nm correspond to out-of-plane quadrupole and in-plane quadrupole plasmon resonance of triangular nanoparticles, respectively. Anisotropic triangular silver nanoparticles are reported³² to have high SERS intensity owing to their three surface plasmon resonance (SPR) bands corresponding to dipole and quadrupole plasmon resonance, while only one SPR band is reported for spherical silver nanoparticles.

HRTEM analysis was performed to investigate the morphology of AgNPs. As shown in Fig. 3, the yellow Ag was found to have spherical shape of nanoparticles with an average diameter of 25 ± 5 nm. Blue Ag was however a mixture of spherical as well as triangular nanoparticles as was observed in UV spectrum. The average dimension of nanoparticles was estimated as 40 ± 20 nm.

Adsorption studies using non-porous and mesoporous silica

Adsorption kinetic experiments were performed for different dye concentrations *i.e.* 50, 100 and 200 mg L⁻¹ with 0.1 g L⁻¹ of SiO₂ and MS-SiO₂. The pseudo-second-order models were applied in order to understand adsorption mechanism. The expression for pseudo-second-order kinetic model is shown in eqn (1) where, q_e (mg g⁻¹) and q_t (mg g⁻¹) are the amounts of dye adsorbed at equilibrium and dye adsorbed at time t , respectively.

$$\frac{t}{q_t} = \frac{1}{k_a q_e^2} + \left(\frac{1}{q_e}\right) t \quad (1)$$

k_a is the equilibrium rate constant of pseudo-second order adsorption (g mg⁻¹ min⁻¹). The slope and intercept of the plot

of $\frac{t}{q_t}$ versus t were used to calculate the rate constant k_a (Fig. 4).

The pseudo first order model was fitted to calculate the value of equilibrium dye concentration $q_{e, \text{Cal}}$ and adsorption equilibrium rate constant k_a . The obtained values of k_a and $q_{e, \text{Cal}}$ for different dye concentrations are mentioned in Table 1.

The $q_{e, \text{Cal}}$ values matches well with the experimental equilibrium dye concentration $q_{e, \text{Exp}}$ values. The k_a values reduced from 2.21 to 1.45 (g mg⁻¹ min⁻¹) and 3.92 to 1.80 (g mg⁻¹ min⁻¹) in non-porous and mesoporous silica respectively with an increase in dye concentration from 50 to 200 mg L⁻¹.

This trend may be explained by the fact that at lower concentrations, a maximum number of dye molecules would be able to get adsorbed on silica surface, ensuring a higher adsorption. By contrast, at higher dye concentrations, a lower adsorption has been monitored due to the saturation of active adsorption sites. The k_a values were found to be higher for mesoporous silica as compared to non-porous silica for all concentrations of dye. It may be inferred from the results that high porosity and large surface area of microporous silica facilitates the adsorption of methylene blue.

FTIR analysis was carried out to investigate the interaction of methylene blue with mesoporous silica nanoparticles leading to its strong adsorption. As shown in Fig. 5, the peak at 800 and 3000–3700 cm⁻¹ corresponding to symmetric stretching of Si–O–Si and –OH respectively were found to be broadened. The broadening of peaks indicates interaction of –OH of silica nanoparticles with methylene blue. Further, the peak corresponding to asymmetric stretching of Si–O–Si at 1050–1150 cm⁻¹ disappeared indicating the adsorption of dye molecules on MS-SiO₂ nanoparticles.³³ The adsorption of dye also resulted in disappearance of –NH stretching peak at 1633 cm⁻¹ and enhancement of –C=C stretching at 1635 cm⁻¹ due to adsorbed dye molecules. It may therefore be inferred that in addition to porous nature and large surface area, amino and hydroxyl group present on the surface of silica nanoparticles are likely to have weak hydrogen bonding with the dye molecules. This interaction

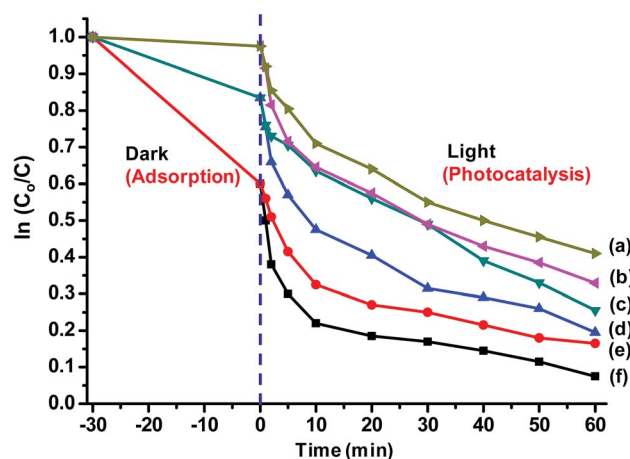


Fig. 9 Photocatalytic behaviour of (a) yellow Ag (b) blue Ag (c) SiO₂/yellow Ag (d) SiO₂/blue Ag (e) MS-SiO₂/yellow Ag and (f) MS-SiO₂/blue Ag.



Table 2 Degradation rate constant k_d values of Ag and SiO₂/Ag composite nanostructures

Samples	k_d (g mg ⁻¹ min ⁻¹) × 10 ⁻³
Yellow Ag	16.3 ($R^2 = 0.978$)
Blue Ag	19.3 ($R^2 = 0.901$)
SiO ₂ /yellow Ag	19.9 ($R^2 = 0.878$)
SiO ₂ /blue Ag	25.1 ($R^2 = 0.86$)
MS-SiO ₂ /yellow Ag	26.3 ($R^2 = 0.822$)
MS-SiO ₂ /blue Ag	31.3 ($R^2 = 0.842$)

facilitates the strong adsorption of dye on the surface of mesoporous silica nanoparticles as shown in Scheme 2.

Morphology of SiO₂/Ag composite nanostructures

SiO₂ offers surface for adsorption of dye molecules, AgNPs, on the other hand, act as a good photocatalytic agent. HRTEM analysis of SiO₂/Ag and MS-SiO₂/Ag composite nanostructures are shown in Fig. 6 and 7 respectively. The AgNPs are clearly visible on the surface of SiO₂ nanoparticles. The shape of AgNPs is spherical in case of SiO₂/yellow Ag composite nanostructures while a mixture of spherical as well as triangular AgNPs was noticed in SiO₂/blue Ag composite nanostructures.

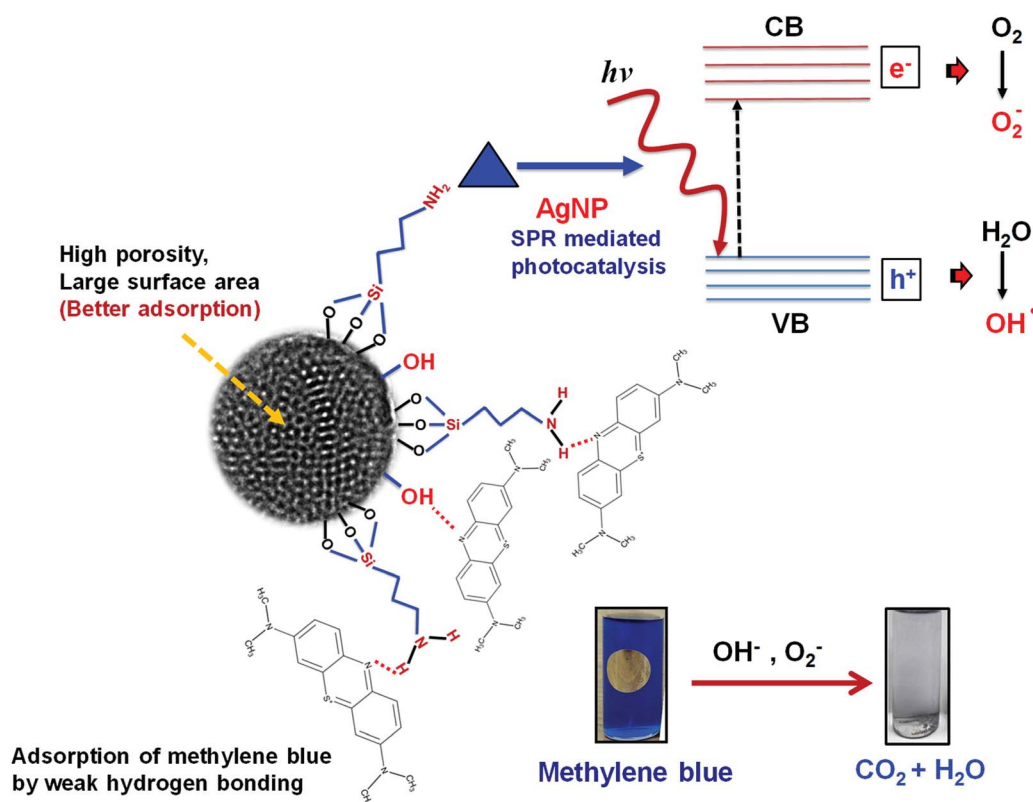
The presence of Ag in MS-SiO₂/blue Ag composite nanostructure was further confirmed by EDX (Energy Dispersive X-ray) analysis (Fig. 8). The EDX mapping results showed homogenous distribution of AgNPs was observed. The triangular shape of AgNPs was also confirmed by EDX mapping.

Photocatalytic behavior of SiO₂/Ag composite nanostructures

0.2% (w/v) of Ag and SiO₂/Ag composite nanostructures were compared for their photocatalytic activity. The nanoparticles were dispersed in dye solution (0.02% w/v) and placed in dark for 30 min to achieve adsorption–desorption equilibrium followed by exposure to sunlight and analysis of their photocatalytic behaviour.

The dye degradation behaviour of various nanostructures is shown in Fig. 9. The dye degradation was observed in all nanostructures, however, the extent of dye degradation was found to be a function of morphology of silica as well as AgNPs. The blue AgNPs exhibited ~18% higher degradation as compared to yellow AgNPs. The triangular nanoparticles had two peaks in UV spectra indicating efficient SPR, which resulted in generation of larger number of reactive species leading to better dye degradation. The non-porous SiO₂/Ag composite nanostructures were found to possess better photocatalysis behaviour as compared to pristine AgNPs. This may be attributed to adsorption of dye as evident from k_a values already shown in Table 1.

They also assisted in better dispersion of AgNPs on their surface leading to improved SPR mediated photocatalysis. The k_d values for SiO₂/yellow Ag and SiO₂/blue Ag composite nanostructures were estimated as 19.9×10^{-3} and 25.1×10^{-3} g mg⁻¹ min⁻¹ respectively with an improvement of 22 and 30% compared to pristine AgNPs. The photocatalysis behaviour was further enhanced in the case of Ag decorated mesoporous SiO₂ nanostructures. MS-SiO₂/yellow Ag composite nanostructures were found to have k_d value of 26.3×10^{-3} g mg⁻¹ min⁻¹ with

**Scheme 3** Photocatalytic mechanism of MS-SiO₂/blue Ag composite nanostructures.

an improvement of 61% compared to yellow AgNPs. MS-SiO₂/blue Ag nanostructures, owing to better SPR mediated photocatalytic activity exhibited even better k_d value of $31.3 \times 10^{-3} \text{ g mg}^{-1} \text{ min}^{-1}$ (Table 2).

The porous nature and large surface area of MS-SiO₂/Ag composite nanostructures not only resulted in better adsorption of methylene blue, but also showed higher photocatalytic degradation (improvement of 62% in k_d value) due to surface plasmon mediated photocatalysis by triangular silver nanoparticles. It may therefore be deduced from the results that large surface area and porosity of mesoporous silica nanoparticles along with enhanced SPR of triangular AgNPs make them good adsorbing material as well as efficient photocatalyst. The proposed mechanism of photodegradation is shown in Scheme 3.

Conclusions

Non-porous and mesoporous silica nanoparticles were synthesized successfully and characterized using SEM and HRTEM. The estimated pore size of mesoporous silica NPs was found to be 3.2 nm. The adsorption behavior of amine functionalized non-porous and mesoporous silica nanoparticles was compared. The pseudo first order model was fitted to calculate the value of equilibrium dye concentration $q_{e \text{ Cal}}$ and adsorption equilibrium rate constant k_a . The $q_{e \text{ Cal}}$ values were found to match fairly well with the experimental equilibrium dye concentration $q_{e \text{ Exp}}$ values. The increase in dye concentration from 50 to 200 mg L⁻¹ resulted in decrease in k_a values from 2.21 to 1.45 (g mg⁻¹ min⁻¹) and 3.92 to 1.8 (g mg⁻¹ min⁻¹) for non-porous and mesoporous silica respectively. The high porosity and large surface area of mesoporous silica facilitated the adsorption of methylene blue on its surface and the k_a values were found to be higher for mesoporous silica as compared to non-porous silica for all the concentrations of dye. Ag decorated SiO₂ nanoparticles were successfully synthesized by attaching yellow and blue AgNPs on the surface of amine functionalized silica. The photocatalytic activity of the mesoporous SiO₂/Ag was compared with that of non-porous SiO₂/Ag nanoparticles and pristine Ag nanoparticles. Mesoporous SiO₂/Ag nanoparticles showed remarkable improvement in rate of degradation of methylene blue as compared to non-porous SiO₂ and pristine Ag nanoparticles respectively. Blue Ag nanoparticles, owing to their better charge carrier generation and enhanced surface plasmon resonance, exhibited better photocatalysis performance as compared to yellow Ag nanoparticles among all the nanostructures. Large surface area and high porosity of mesoporous silica nanoparticles in combination with surface plasmon resonance of blue Ag contributed to significant improvement in photocatalysis of SiO₂/Ag composite nanostructures.

Conflicts of interest

There are no conflicts to declare.

Acknowledgements

The authors would like to thank Bhaskaracharya College of Applied Sciences for providing the Laboratory facilities.

Notes and references

- 1 N. Jain, R. Singh, G. Kumar, B. Pani, R. Nain, K. Dutt, P. K. Muwal and S. Sirohi, *ChemistrySelect*, 2017, 2, 11415–11421.
- 2 S. M. Rafigh and A. Heydarinasab, *ACS Sustainable Chem. Eng.*, 2017, 5, 10379–10386.
- 3 K. Gude, V. M. Gun'ko and J. P. Blitz, *Colloids Surf., A*, 2008, 325, 17–20.
- 4 H. Wang and Y. Huang, *J. Hazard. Mater.*, 2011, 191, 163–169.
- 5 B. Hameed, A. M. Din and A. Ahmad, *J. Hazard. Mater.*, 2007, 141, 819–825.
- 6 R. Han, J. Zhang, P. Han, Y. Wang, Z. Zhao and M. Tang, *Chem. Eng. J.*, 2009, 145, 496–504.
- 7 G. Wu, A. Koliadima, Y.-S. Her and E. Matijević, *J. Colloid Interface Sci.*, 1997, 195, 222–228.
- 8 Y. Chen, in *Design, Synthesis, Multifunctionalization and Biomedical Applications of Multifunctional Mesoporous Silica-Based Drug Delivery Nanosystems*, Springer, 2016, pp. 31–46.
- 9 L. Tang and J. Cheng, *Nano Today*, 2013, 8, 290–312.
- 10 U. K. Sharma, M. Kushwaha, H. Tiwari and A. Prakash, *World J. Pharm. Pharm. Sci.*, 2014, 11, 257–271.
- 11 X. Huang, N. P. Young and H. E. Townley, *Nanomater. Nanotechnol.*, 2014, 4, 2–15.
- 12 G. Zhang, J. Gao, J. Qian, L. Zhang, K. Zheng, K. Zhong, D. Cai, X. Zhang and Z. Wu, *ACS Appl. Mater. Interfaces*, 2015, 7, 14192–14200.
- 13 C. Bharti, U. Nagaich, A. K. Pal and N. Gulati, *Int. J. Pharm. Invest.*, 2015, 5, 124.
- 14 C. Argyo, V. Weiss, C. Bräuchle and T. Bein, *Chem. Mater.*, 2013, 26, 435–451.
- 15 S. Sharmiladevi, A. S. Priya and M. Sujitha, *Int. J. Pharm. Pharm. Sci.*, 2016, 8, 196–201.
- 16 L. Cao, H. Zhang, C. Cao, J. Zhang, F. Li and Q. Huang, *Nanomaterials*, 2016, 6, 126.
- 17 A. Krysztalkiewicz, S. Binkowski and T. Jesionowski, *Appl. Surf. Sci.*, 2002, 199, 31–39.
- 18 J. Schneider, M. Matsuoka, M. Takeuchi, J. Zhang, Y. Horiuchi, M. Anpo and D. W. Bahnemann, *Chem. Rev.*, 2014, 114, 9919–9986.
- 19 E. S. Elmolla and M. Chaudhuri, *J. Hazard. Mater.*, 2010, 173, 445–449.
- 20 G. Bandekar, N. Rajurkar, I. Mulla, U. Mulik, D. Amalnerkar and P. Adhyapak, *Appl. Nanosci.*, 2013, 4, 199.
- 21 S. Li, Z. Ma, L. Wang and J. Liu, *Sci. China, Ser. B: Chem.*, 2008, 51, 179–185.
- 22 Y. Badr and M. Mahmoud, *J. Phys. Chem. Solids*, 2007, 68, 413–419.
- 23 X. Chen, Z. Zheng, X. Ke, E. Jaatinen, T. Xie, D. Wang, C. Guo, J. Zhao and H. Zhu, *Green Chem.*, 2010, 12, 414–419.
- 24 K. Aslan, M. Wu, J. R. Lakowicz and C. D. Geddes, *J. Fluoresc.*, 2007, 17, 127–131.



- 25 A. Nimrodh Ananth, S. Umapathy, J. Sophia, T. Mathavan and D. Mangalaraj, *Appl. Nanosci.*, 2011, **1**, 87–96.
- 26 J. Alimunnisa, K. Ravichandran and K. S. Meena, *J. Mol. Liq.*, 2017, **231**, 281–287.
- 27 W. Wang, Z. Li, B. Gu, Z. Zhang and H. Xu, *ACS Nano*, 2009, **3**, 3493–3496.
- 28 K. H. Chen, Y. C. Pu, K. D. Chang, Y. F. Liang, C. M. Liu, J. W. Yeh, H. C. Shih and Y. J. Hsu, *J. Phys. Chem. C*, 2012, **116**, 19039–19045.
- 29 S. Sirohi, A. Singh, C. Dagar, G. Saini, B. Pani and R. Nain, *Appl. Nanosci.*, 2017, 1–11.
- 30 G. Castruita-de León, Y. A. Perera-Mercado, L. A. García-Cerda, J. A. Mercado-Silva, H. I. Meléndez-Ortiz, Y. Olivares-Maldonado and L. Alvarez-Contreras, *Microporous Mesoporous Mater.*, 2015, **204**, 156–162.
- 31 Q. Zhang, J. Ge, T. Pham, J. Goebel, Y. Hu, Z. Lu and Y. Yin, *Angew. Chem.*, 2009, **121**, 3568–3571.
- 32 L. Lu, A. Kobayashi, K. Tawa and Y. Ozaki, *Chem. Mater.*, 2006, **18**, 4894–4901.
- 33 H. T. Lu, *Colloid J.*, 2013, **75**, 311–318.

